ANNUAL REVIEWS

Annual Review of Fluid Mechanics

Capillarity in Soft Porous Solids

Jonghyun Ha and Ho-Young Kim

Department of Mechanical and Aerospace Engineering, Seoul National University, Seoul 08826, Korea; email: hyk@snu.ac.kr

ANNUAL REVIEWS CONNECT

www.annualreviews.org

- Download figures
- Navigate cited references
- Keyword search
- Explore related articles
- Share via email or social media

Annu. Rev. Fluid Mech. 2020. 52:263–84

First published as a Review in Advance on August 19, 2019

The *Annual Review of Fluid Mechanics* is online at fluid.annualreviews.org

https://doi.org/10.1146/annurev-fluid-010518-040419

Copyright © 2020 by Annual Reviews. All rights reserved

Keywords

capillarity, poroelasticity, swelling, morphing

Abstract

Soft porous solids can change their shapes by absorbing liquids via capillarity. Such poro-elasto-capillary interactions can be seen in the wrinkling of paper, swelling of cellulose sponges, and morphing of resurrection plants. Here, we introduce physical principles relevant to the phenomena and survey recent advances in the understanding of swelling and shrinkage of bulk soft porous media due to wetting and drying. We then consider various morphing modes of porous sheets, which are induced by localized wetting and swelling of soft porous materials. We focus on physical insights with the aim of triggering novel experimental findings and promoting practical applications.

1. INTRODUCTION

Capillarity broadly refers to the interfacial interaction between liquid and fluid (gas or immiscible liquid) arising from cohesion within the liquid (de Gennes et al. 2004). When another phase (solid) is additionally involved, the question is how the liquid–fluid interface will be shaped and move on the solid surface, leading to the study of wetting (de Gennes 1985). A canonical problem of wetting deals with the liquid rise into a vertical capillary, as shown in **Figure 1*a***. Its statics were first quantitatively studied by Boyle (1662), followed by Jurin (1718), who determined the functional dependence of the rise height on the geometric parameters. Bell & Cameron (1906), Lucas (1918), and Washburn (1921) studied the dynamics of liquid imbibition in capillaries. More recently, the rise of a liquid between flexible lamellae, as shown in **Figure 1*b***, was analyzed (Bico et al. 2004, Kim & Mahadevan 2006), which provoked the study of capillarity coupled with flexible solids like rods (Duprat et al. 2012, Sojoudi et al. 2017), plates (Py et al. 2007, Paulsen et al. 2015), and tubes (Hoberg et al. 2014). Recent developments in this field, termed elasto-capillarity, have been reviewed by Bico et al. (2018).

In contrast, for a cracker dipped into coffee (**Figure 1*c***) (Fisher 1999), we need to go beyond classical elasto-capillarity to understand the dynamics of wetting, swelling, and softening of this mundane piece of food. The wetting of soft porous solids (e.g., foods, paper, sponges, hydrogels) gives rise to strain, stress, and changes in the properties of the solid structure that surrounds the voids being filled with liquid. Therefore, the theory of poroelasticity (Wang 2000) needs to be coupled with capillarity in the context of poro-elasto-capillarity (Ha et al. 2018, Nasouri et al. 2019).

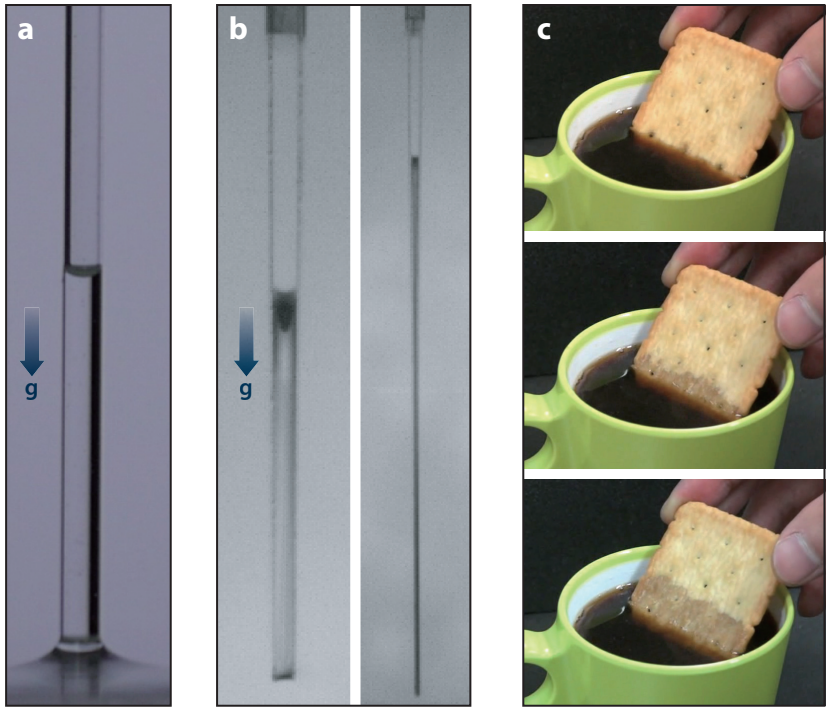

Figure 1

(*a*) The rise of water in a rigid glass capillary. (*b*) The rise of water between flexible coverslips of glass. (*c*) A cracker dipped into coffee. Panel *b* adapted from Kim & Mahadevan (2006).

The study of the elastic deformation of poroelastic materials due to fluid pressure change or fluid injection in their pores began almost a century ago by Terzaghi (1925) and then was later continued by Biot (1941). Since Tanaka & Fillmore (1979) theoretically investigated the coupling between swelling and spontaneous fluid infiltration of poroelastic media, significant advances have been made in the understanding of absorption and expansion of dense porous media, such as gels (Doi 2009, Yoon et al. 2010, Bertrand et al. 2016) and matrices of dense absorbent materials (Sweijen et al. 2017). In addition to wetting and swelling, the drying of initially wet poroelastic media has been studied to understand their shrinkage and cracking behavior (Wittmann 1976, Scherer 1989). Interest in the capillary interaction of liquids with a variety of soft porous materials is ever growing, driven by its relevance to geophysics (Style et al. 2011, Laloui et al. 2016), biology (Dawson et al. 1997, Skotheim & Mahadevan 2005, Dumais & Forterre 2012), and biologically inspired engineering (Chen et al. 2014) and by its novel applications to soft actuation and robotics (Hines et al. 2017, Hu et al. 2018).

Here, we review fundamental physical principles and recent advances associated with deformations of soft porous solids induced by capillarity. Our review aims to serve as a quick guide to the discipline, which has been investigated almost independently in each of the diverse fields of materials science, geophysics, nanotechnology, biology, and rheology. We start from the physical principles of classical imbibition dynamics and then move on to introduce the theoretical framework of the general responses of soft porous solids to liquid invasion. Next, we categorize recent advances in the understanding of poro-elasto-capillary phenomena according to the geometrical characteristics of the systems. We begin with the swelling and shrinkage of bulk soft porous solids under the effects of capillarity. Then we consider various morphing modes of porous sheets, which are induced by localized swelling of soft porous materials due to wetting. We focus on physical insights, rather than focusing on mathematical details or providing an exhaustive literature survey, with the aim of triggering advances from experimentalists and promoting further practical applications.

2. PHYSICAL PRINCIPLES OF CAPILLARITY IN RIGID POROUS SOLIDS

2.1. Classical Models of Imbibition in Capillaries

Porous solids with voids filled with a gas are impregnated by a liquid when the void surfaces prefer contact to the liquid over the gas. The affinity of a solid surface to a liquid surrounded by a gas is often measured by the equilibrium contact angle, which obeys Young's (1805) equation when the solid is sufficiently rigid (Adam 1930, Park et al. 2014). The dynamic process of reducing the free energy (Adamson & Gast 1997) of the gas–liquid–porous solid system is classically understood using the so-called Washburn equation (Bell & Cameron 1906, Lucas 1918, Washburn 1921). Modeling porous networks as an assemblage of narrow capillaries, we consider the velocity of the liquid front in a wettable capillary of radius R, as shown in **Figure 2*a***, where a liquid reservoir contacts one end of the capillary. If γ is the liquid–gas surface tension coefficient and L is the wetted length, the wall shear stress τ is estimated as $\tau \sim \eta \dot{L}/R$, where η is the liquid viscosity and the overdot denotes the time derivative. When inertia is negligible relative to viscous forces, the driving capillary force, $F_\mathrm{d} \sim \gamma R$, is balanced by the resisting viscous force, $F_\mathrm{r} \sim \tau RL$. Here, we have assumed that the viscous dissipation in the bulk of length L is much larger than the dissipation in the wedge near the advancing contact line (de Gennes 1985, Kim 2007). The result yields the classical diffusive behavior of the wetted length with time t, $L \sim (\gamma Rt/\eta)^{1/2} = (D_\mathrm{w} t)^{1/2}$, where $D_\mathrm{w} = \gamma R/\eta$ is the dynamic coefficient for capillary wicking.

An important aspect of this seemingly simple rule is that a single geometric scale, R, determines the wicking velocity. This implies that the variation of the radius of a capillary may cause $L(t)$ to

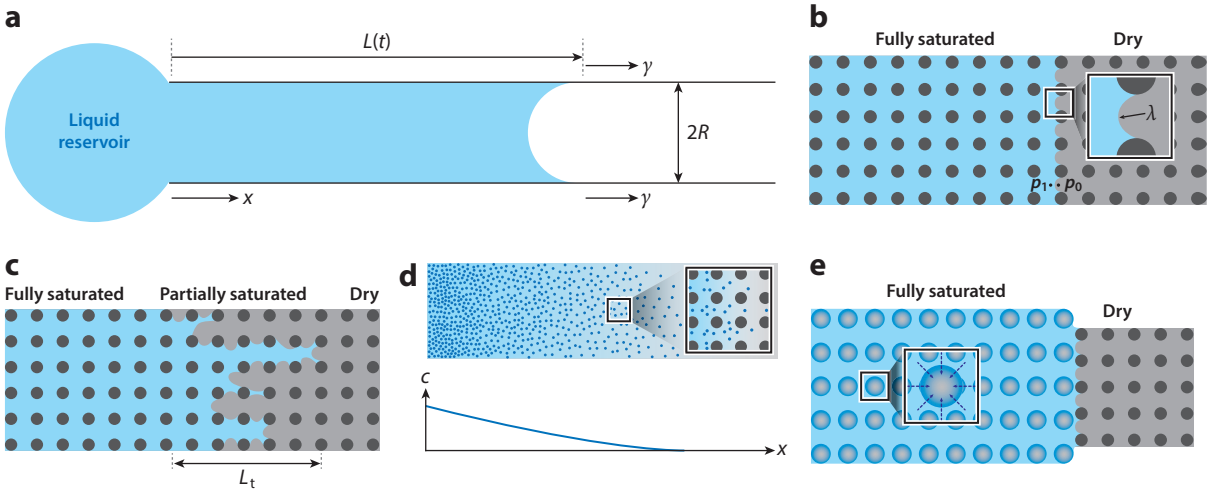

Figure 2

(*a*) A schematic of liquid imbibition into a horizontal capillary with a contact angle of zero. (*b*) A schematic of liquid imbibition into a porous medium with a sharp liquid–gas interface. (*Inset*) A liquid meniscus with the characteristic radius of curvature. (*c*) A schematic of the partially saturated transition zone between the fully saturated and dry zones. (*d*) A diffusive transition region exhibiting a smooth change of molecular concentration. (*e*) A porous medium consisting of hygroscopically active skeletons that swell upon wetting. (*Inset*) A hygroscopically active skeleton that absorbs the surrounding liquid. Abbreviations: c, molecular concentration; L, wetted length; L_t, partially saturated zone length; p, pressure; R, capillary radius; γ, liquid–gas surface tension coefficient; λ, characteristic radius of curvature.

deviate from the classical rule, in particular by changing the exponent of time, as has been explored in diverse settings (Reyssat et al. 2008, Gorce et al. 2016, Liu et al. 2018). The diffusive rule also holds for hemiwicking, the wetting of porous surfaces by a liquid film (Bico et al. 2001), although it is more complicated owing to multiple, rather than single, geometric factors, including the height and spacing of protrusions and the surface roughness (Kim et al. 2011, 2016). In the following, we consider liquid flows in porous media that cannot simply be assumed to be an assemblage of capillaries.

2.2. Darcy's Law and Unsaturated Media

Fluid flows in porous media with negligible inertia are described by Darcy's law (Darcy 1856, Adler & Brenner 1988),

$$\mathbf{q} = -\frac{k}{\eta}\nabla\Psi, \qquad 1.$$

where $\mathbf{q}$ is the volume flux and Ψ is the potential for liquid flow, corresponding to the pressure p in pressure-driven flows. The permeability k roughly corresponds to the cross-sectional area of the fluid conduit that generates viscous dissipation in a porous medium (Childs & Collis-George 1950, Kim et al. 2017), although it also depends on the configuration of the fluid paths (Bear 1972, Xu & Yu 2008).

We first apply Darcy's law to the capillary imbibition with a sharp liquid–gas interface, corresponding to **Figure 2*b***. The pressure difference established between the reservoir and just inside the advancing meniscus is equal to the Laplace pressure, $\Delta p_L = p_0 - p_1 \sim \gamma/\lambda$, where λ is the radius of curvature of the front meniscus. Here, the hydrostatic pressure is assumed to be negligible

compared with the Laplace pressure. Then the wetting velocity, or the average flow velocity, v, is scaled as $v \sim \gamma k/(\eta\lambda L)$. If k and λ are constant along the fluid path and with time, the diffusive rule for L still holds by taking $v = \dot{L}$,

$$L \sim (D_{\mathrm{w}} t)^{1/2}, \qquad 2.$$

where $D_{\mathrm{w}} = \gamma k/(\eta\lambda)$ is the dynamic coefficient for wicking. Assuming $k \sim R^2$ and $\lambda \sim R$ for a straight tube, one recovers the scaling of Washburn's equation. The diffusive rule for the propagation of the wetting front is invalid when the pore size distribution or the liquid content in pores varies spatially, causing changes in k or λ along the fluid path and time (Reyssat et al. 2009, Bal et al. 2011, Ponomarenko et al. 2011, Obara & Okumura 2012, Kim et al. 2017).

In a partially saturated zone of length L_{t}, as shown in **Figure 2*c***, where pores contain gas as well as liquid, the mass conservation equation is written as

$$\frac{\partial \theta}{\partial t} = -\nabla \cdot \mathbf{q}. \qquad 3.$$

Here, the moisture content θ denotes the volume fraction of liquid in a representative volume element scale, which is much greater than individual microscopic pores (Cuerto-Felgueroso & Juanes 2008). The quantity θ can be measured by gravimetric sampling (Hall & Tse 1986), the method of gamma ray attenuation (Nielsen 1972), or nuclear magnetic resonance imaging (Gummerson et al. 1979, Song et al. 2011). Combining Equations 1 and 3 gives (Richards 1931)

$$\frac{\partial \theta}{\partial t} = \nabla \cdot (D_{\mathrm{u}} \nabla \theta), \qquad 4.$$

where the diffusivity, $D_{\mathrm{u}} = (k/\eta)\partial_\theta \Psi$, like Ψ, depends on θ, γ, k, η, and the meniscus curvature in individual pores. In addition to capillarity, Ψ may involve the effects of liquid adsorption to solid surfaces caused by electrostatic and van der Waals forces in partially saturated zones (Philip 1970, Or et al. 2005). Therefore, the moisture content in the partially saturated region follows the diffusion equation, with the diffusivity dependent on the properties of the liquid and the porous network.

The diffusion of the moisture in the unsaturated zone should be distinguished from the molecular diffusion of vapor, as depicted in **Figure 2*d***. The spontaneous transport of vapor in porous media occurs near the wetting front of liquids with high vapor pressure or when the media are surrounded by humid air. Additionally, a medium with very fine pores (e.g., nanometric pores) of poor connectivity may allow only vapor transport because a continuous stream of internal liquid is unlikely. The molecular concentration c of vapor follows the diffusion equation

$$\frac{\partial c}{\partial t} = D_{\mathrm{m}} \nabla^2 c, \qquad 5.$$

owing to Fick's law. Here, D_{m} is the effective diffusivity, a function of the porosity (ϕ) and the vapor diffusivities in the air and in the solid (Kalnin & Kotomin 1998, Shin et al. 2018).

3. PHYSICAL PRINCIPLES OF POROELASTIC RESPONSES TO LIQUID INVASION

3.1. Classical Poroelasticity of Saturated Media

We introduce governing equations to find the fields of displacement, stress, pressure, and amount of fluid in a fully saturated poroelastic medium. In saturated poroelastic media, a change in applied stress causes a change in fluid pressure or fluid mass, and a change in fluid pressure or fluid

mass causes a change in the volume of the porous material (Wang 2000). These couplings lead to the constitutive equations of linear poroelasticity, which relate the stress σ_{ij} and the increment of fluid content ζ to the pressure p and the strain $\epsilon_{ij} = \frac{1}{2}(\partial u_i/\partial x_j + \partial u_j/\partial x_i)$, where u_i is the displacement,

$$\epsilon_{ij} = \frac{1}{2G}\left(\sigma_{ij} - \frac{\nu}{1+\nu}\sigma_{kk}\delta_{ij}\right) + \frac{\alpha}{3K}p\delta_{ij}, \tag{6.}$$

$$\zeta = \frac{\alpha}{K}\frac{\sigma_{kk}}{3} + \frac{\alpha}{KB}p. \tag{7.}$$

Here, G and K are respectively the shear and the bulk modulus, ν is Poisson's ratio, δ_{ij} is the Kronecker delta, α is the Biot–Willis coefficient, and B is Skempton's coefficient. For an incompressible solid and fluid, we have $\alpha = B = 1$. The increment of fluid content ζ is defined as $\zeta = \delta m_{\mathrm{f}}/\rho_{\mathrm{f}}$, where δm_{f} is the change in fluid mass content per unit reference volume and ρ_{f} is the fluid density in the reference state. The force equilibrium dictates

$$\frac{\partial \sigma_{ij}}{\partial x_j} + f_i = 0, \tag{8.}$$

where f_i is the body force per unit bulk volume. Lastly, the continuity equation, $\partial_t \zeta = -\nabla \cdot \mathbf{q}$, combined with Darcy's law (Equation 1) gives

$$\frac{\partial \zeta}{\partial t} = \frac{k}{\eta}\nabla^2 p. \tag{9.}$$

These governing equations allow us to obtain the deformation, stress, fluid pressure, and amount of fluid in isotropic linear poroelastic materials responding to pertinent boundary and initial conditions. For a formal introduction to the basic theory of poroelasticity, readers are referred to the pioneering paper of Biot (1941) and relevant books (Wang 2000, Cheng 2016).

It is interesting to see that substituting Equation 7 in Equation 9 leads to the diffusion equation for p for $\sigma_{kk} = 0$ or $\dot{\sigma}_{kk} = 0$,

$$\frac{\partial p}{\partial t} = D_{\mathrm{p}}\nabla^2 p, \tag{10.}$$

where $D_{\mathrm{p}} = (k/\eta)(KB/\alpha)$ is the poroelastic diffusivity. Additionally, ζ satisfies the diffusion equation $\partial_t \zeta = D_{\mathrm{p}}\nabla^2\zeta$ for $\sigma_{kk} = 0$ or $\nabla^2\sigma_{kk} = 0$. For a system of characteristic length L, the time for the diffusive equilibration of pressure via fluid transport in soft wet media, or the poroelastic time, is given by $\tau_{\mathrm{p}} = L^2/D_{\mathrm{p}} \sim \eta L^2/(kK)$ (Skotheim & Mahadevan 2005). If the timescale of interest to describe a system's dynamic behavior is τ, poroelasticity will govern the dynamics for $\tau \sim \tau_{\mathrm{p}}$. Classical Hookean elasticity suffices for both $\tau \ll \tau_{\mathrm{p}}$ and $\tau \gg \tau_{\mathrm{p}}$, with the elastic modulus hardly changed in the former case but reduced to a softened state in the latter (Skotheim & Mahadevan 2004).

3.2. Poroelasticity of Gels

Gels are cross-linked networks of polymers or colloids within a liquid (solvent). They can allow the liquid to move within the network while behaving like a soft solid (Flory 1953). Unlike the classical porous flows considered above, fluid transport in gels is driven by the difference of chemical potential rather than pressure. The flux $\mathbf{J}$ of the solvent driven by the gradient of the chemical potential μ is described by Darcy's law of the form (Wijmans & Baker 1995,

Hu et al. 2010) $\mathbf{J} = -k/(\eta\Omega^2)\nabla\mu$, where Ω is the volume per solvent molecule. The solvent flux gives rise to a change of concentration C of the solvent in the gel, satisfying the continuity equation $\partial_t C = -\nabla \cdot \mathbf{J}$. Combining the continuity equation and Darcy's law, we get

$$\frac{\partial C}{\partial t} = \frac{k}{\eta\Omega^2}\nabla^2\mu. \qquad 11.$$

The constitutive equation that relates the stress to the strain and chemical potential is written as (Doi 2009, Yoon et al. 2010)

$$\sigma_{ij} = 2G\left(\epsilon_{ij} + \frac{\nu}{1-2\nu}\epsilon_{kk}\delta_{ij}\right) - \frac{\mu-\mu_0}{\Omega}\delta_{ij}, \qquad 12.$$

where μ_0 is the chemical potential in the reference state. The quantity $(\mu - \mu_0)/\Omega$ corresponds to the pore pressure in Equation 6, in which we took $\alpha = 1$ for incompressible network polymers and solvent molecules. The increase of the gel volume is related to the concentration as

$$\epsilon_{kk} = \Omega(C - C_0), \qquad 13.$$

where C_0 is the concentration in the reference state. Equations 11–13, combined with the force equilibrium Equation 8, allow us to find the displacement, stress, chemical potential, and solvent concentration under pertinent boundary and initial conditions.

It can be shown that the concentration profile obeys the diffusion equation, $\partial_t C = D_\mathrm{p}\nabla^2 C$. Here, the poroelastic diffusivity D_p of a gel is given by $D_\mathrm{p} \sim Gk/\eta$ (Johnson 1982, Hu et al. 2010), consistent with the abovementioned D_p of classical poroelasticity. For the diffusive nature of the solvent transport, the thickness of a rectangular slab, as shown in **Figure 3*a***, initially grows as $(D_\mathrm{p}t)^{1/2}$. The characteristic time for a slab of thickness L to grow to a new equilibrium since the change of the surrounding solvent concentration is given by $\tau_\mathrm{p} = L^2/D_\mathrm{p}$.

3.3. Classification of Soft Porous Solids for Wetting Analysis

While Sections 3.1 and 3.2 have dealt with poroelastic media whose pores are fully saturated with liquid, our major interest in this review is capillary invasion of liquid into gas-filled pore spaces. In addition, the response of a soft porous solid is drastically different depending on the ability of the solid skeleton to swell by absorbing surrounding liquid. The skeleton materials that expand by absorbing water are called hygroscopically active. In this section, we first consider hygroscopically inactive skeletons like soils, rocks, building materials, and glass beads. Then we move on to more complicated cases of hygroscopically active skeletons like beads and scaffolds of hydrogel and cellulose fibers.

Figure 2*b* depicts the spontaneous liquid infiltration of soft porous media consisting of hygroscopically inactive skeletons. If the wetting front is well defined to be at $x = L$, the wetted region, $0 < x < L$, is fully saturated with liquid while the pores are filled with gas for $x > L$. The poroelastic behavior of fully saturated media, as formulated in Section 2.1, arises in the wetted region. The pressure decreases from the atmospheric pressure in the reservoir, p_0, to a lower pressure due to capillarity, $p_1 = p_0 - \Delta p_\mathrm{L}$, where the Laplace pressure Δp_L scales as γ/λ. Then the wetted region should shrink for its negative gauge pressure inside, unless it is fixed to its sides. The shrinkage of pores leads to changes in permeability k and the radius of curvature of front meniscus λ, which should modify D_w in Equation 2. The shrinkage of porous hygroscopically inactive solids with capillary infiltration has mainly been studied in the context of soil aggregation (Ghezzehei & Or 2000). In contrast, shrinkage of soft porous solids due to drying has been the subject of intense

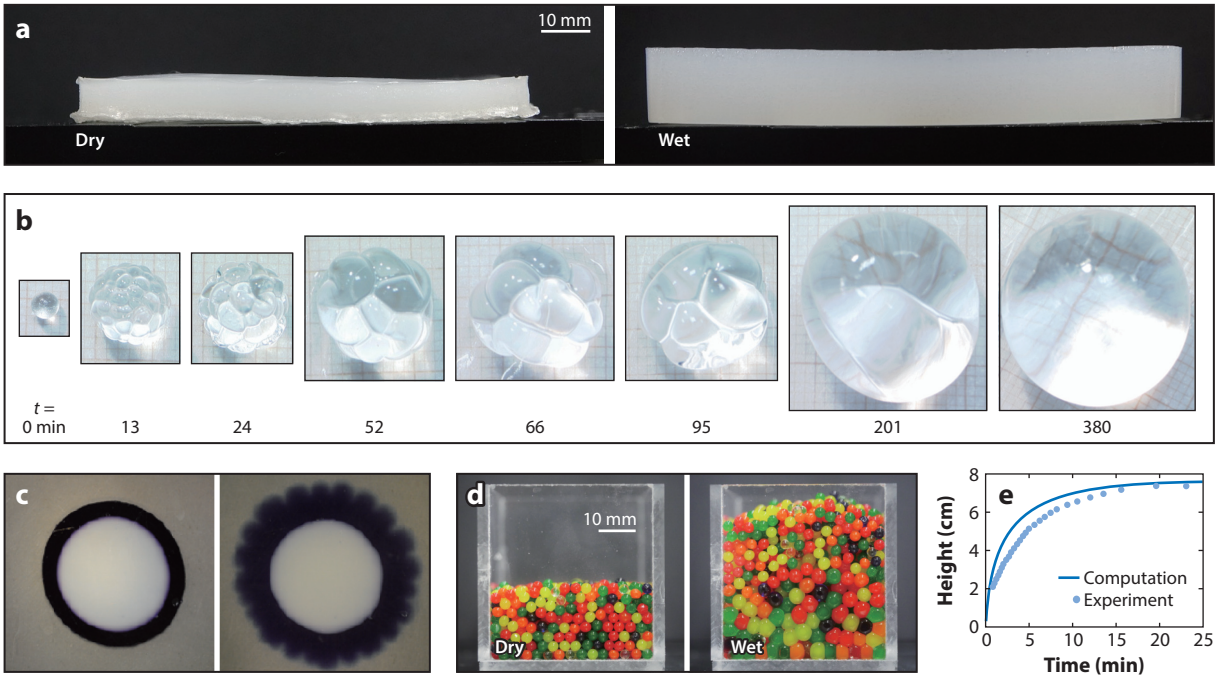

Figure 3

(*a*) A hydrogel slab swelling with the invasion of water. (*b*) A hydrogel sphere swelling with water, exhibiting temporal growth and decay of circumferential lobes. (*c*) A swelling hydrogel ring that wrinkles due to the invasion of water from the outer periphery. (*d*) Vertical expansion of a bed of spherical hydrogels due to contact with water at the bottom. (*e*) Temporal evolution of the height of a bed of superabsorbent polymer particles immersed in water. Panels *b*, *c*, and *e* adapted from Bertrand et al. (2016), Dervaux et al. (2011), and Sweijen et al. (2017), respectively.

study in diverse fields (Bacchin et al. 2018). As the meniscus of the receding liquid develops a large curvature, the force due to negative gauge pressure compresses the solids, which is treated below in a separate section.

Figure 2*c* shows a porous medium of a hygroscopically inactive skeleton, where the liquid meniscus is distributed over a partially saturated, or unsaturated, zone of length L_t between fully saturated and dry regions. The unsaturated zone manifests in the wetting process when the pore structure is heterogeneous or when the driving force for liquid flow is weak (Song et al. 2011). The importance of partial saturation is greater in the drying process, where pinning of gas–liquid–solid contact lines promotes the development of the unsaturated zone (Singh et al. 2019). The widely distributed menisci producing negative gauge pressure tend to strengthen the compressive effect, but this is counteracted by the dry pores in the unsaturated region. One challenge for computational models of unsaturated poroelastic media is to accurately account for capillary forces in individual pores (Coussy 2007, Uzuoka & Borja 2012).

A porous medium of hygroscopically active skeletons is shown in **Figure 2*e***. While wicking into hydrophilic macropores, which are distinct from the nanopores within the skeletons, the liquid is simultaneously absorbed into the skeletons. As the skeletons swell, the entire medium and the macropores expand when subject to no external constraints. The poroelastic responses of the fully saturated zone and of hygroscopically inactive skeletons differ in the following ways. First, liquid sinks are present in the fully saturated zone. If the representative volume element scale is much greater than the macropore scale, the continuity equation reads as $\partial_t \zeta + \nabla \cdot \mathbf{q} = -Q$, where Q is

the volume of liquid entering the skeleton per bulk volume per time. Second, the pore size changes, which makes the effects of solid displacement velocity, $\partial_t \mathbf{u}$, on the flux important and significantly modifies the permeability, k. If a partially saturated zone exists between the fully saturated and dry zones, the physics becomes further involved, as discussed above.

4. CAPILLARY MORPHING OF POROELASTIC BULKS

Capillary imbibition of liquids into initially dry, macroscopic poroelastic media, such as particle beds (Peev & Tzibranska 1997), fiber networks (Karlsson et al. 1998), plant tissues (Rafsanjani et al. 2015b), food (Saguy et al. 2005), paper (Masoodi & Pillai 2010), and cellulose sponges (Ha et al. 2018), can induce volume changes of voids and (hygroscopically active) skeletons, whose combinations morph poroelastic bulks. We first consider the capillary morphing of porous matrices comprising hygroscopically inactive skeletons, which has been primarily studied in the context of drying rather than wetting. We then move on to porous media with hygroscopically active skeletons like gels. Next, we treat hygroscopically active cellulosic materials separately for their peculiar properties.

4.1. Drying, Shrinkage, and Cracking

Drying or dewetting occurs when initially wet porous media are exposed to the surrounding gas. In the ideal linear theory of poroelasticity without considering capillarity, fluid extraction and shrinkage are reverse processes to fluid injection and swelling. This is not the case when considering the effects of capillarity because wetting shrinks the medium of hygroscopically inactive skeletons just as drying does. The nonlinearity introduced by large deformations exhibits significant differences between wetting and drying in the temporal evolutions of size, stress, and pressure. Furthermore, interfacial flows in porous solids can be strongly irreversible because of the pinning of the contact line, contact angle hysteresis (the difference between the advancing and receding contact angles), and the trapping of the retracting liquid within relatively smaller pores, leading to wet islands (Rey & Vandamme 2013, Singh et al. 2019).

Wet porous media shrink with drying as the liquid–gas menisci in the voids generate strong negative gauge pressure (due to loss of liquid). In principle, we can start from the evaporation rate of the wet media, which allows us to find the amount and distribution of remaining liquid through Darcy's law. The pressure, which depends on the curvature of the meniscus in the voids, can be given as $p = p_0 - \gamma\kappa_\mathrm{m}$, where κ_m is the meniscus curvature. We can then find strains using the poroelastic constitutive relation of the stress–strain and force equilibrium, which finally gives the temporal evolution of the shape and size.

Smith et al. (1995) proposed a simple model to obtain the density of shrinking porous media by considering the stress on the solid skeleton, σ_s, that evolves from zero as the bulk density ρ changes from the initial value ρ_0, $\mathrm{d}\sigma_\mathrm{s} = -K\mathrm{d}\rho/\rho$. Here, the dependence of the bulk modulus K on the density can be obtained empirically (Woignier et al. 1989). In the relaxed state, we write $\sigma_\mathrm{s} = (1 - \rho/\rho_\mathrm{s})(p - p_0)$, where ρ_s is the density of the solid phase. This gives ρ as a function of κ_m,

$$\int_{\rho_0}^{\rho} \frac{K(\rho)}{\rho}\,\mathrm{d}\rho - \gamma\kappa_\mathrm{m}\left(1 - \frac{\rho}{\rho_\mathrm{s}}\right) = 0. \qquad 14.$$

Since κ_m is related to the pore size, which in turn can be modeled as a function of the density, we can close Equation 14 to find ρ. It is physically inferred that the density after drying increases with a higher surface tension coefficient (stronger compaction) and a lower bulk modulus (softer skeleton).

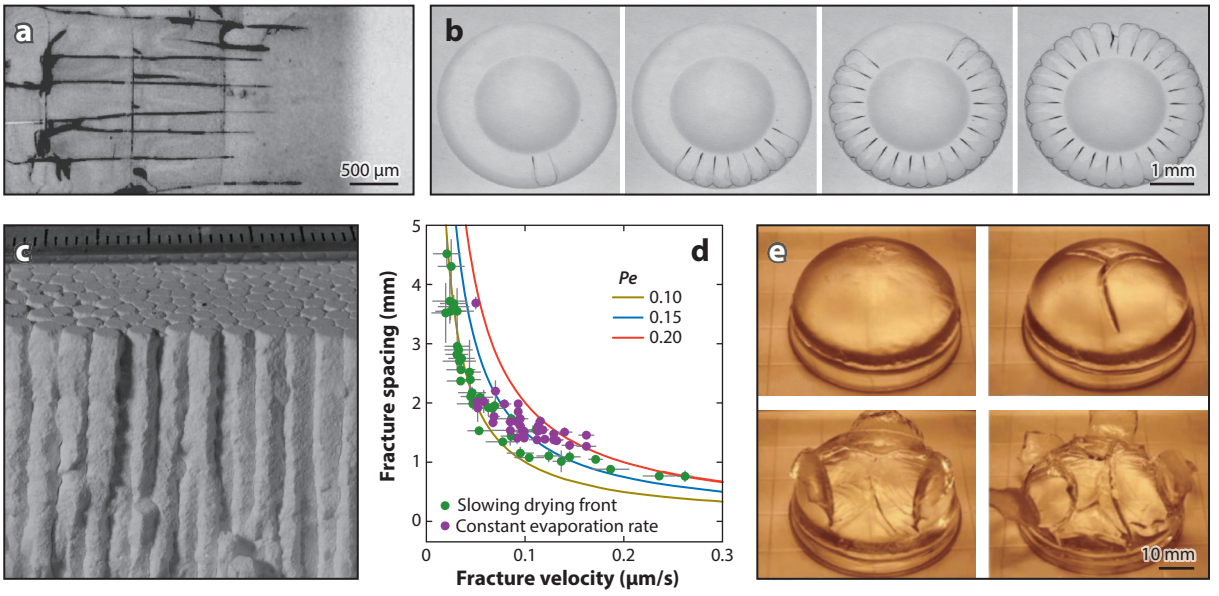

Figure 4

(*a*) Cracks propagating from the drying left side of a silica nanoparticle suspension. (*b*) Cracks at the surface of a drying droplet of a silica nanoparticle suspension. (*c*) Columnar joints arising from the drying of cornstarch. (*d*) The fracture spacing of columnar joints of drying cornstarch plotted against the average fracture advance speed. Circular symbols correspond to experimental measurements, and lines indicate curves of constant Péclet number (*Pe*). (*e*) Cracking and exfoliation of a drying cross-linked PDMS (polydimethylsiloxane) network in hexanes. Panels adapted from (*a*) Dufresne et al. (2006), (*b*) Giorgiutti-Dauphiné & Pauchard (2014), (*c*,*d*) Goehring et al. (2009), and (*e*) Chung et al. (2016).

Surfaces of soft porous media may develop instabilities as their volume changes. Porous media swelling due to liquid invasion develop compression on the fast-swelling outer region, leading to surface corrugations on plates (Tanaka et al. 1992), spheres (Bertrand et al. 2016), and rings (Dervaux et al. 2011), as shown in **Figure 3*b*,*c***. During drying, the liquid loss through the surface tends to shrink the superficial region, which is prevented by the inner core (for thick media) or an adhesive substrate (for a thin film). When the developed tensile stress on the outer layer exceeds a critical value, cracks are generated at the surface, as shown in **Figure 4*a*** for drying deep suspensions (Allain & Limat 1995, Dufresne et al. 2006) and in **Figure 4*b*** for a thin film of a drying colloidal droplet (Giorgiutti-Dauphiné & Pauchard 2014). Such cracks are also found in drying gels (Scherer 1990), paints (Keck 1969), bloodstains (Bou Zeid et al. 2013), and muds (Kindle 1917).

The spacing between cracks, Λ, can be regarded as a characteristic horizontal distance over which the pressure near the outer surface reaches the critical value, p_c, and then relaxes. Darcy's law gives a scaling for Λ as $\Lambda \sim (k/\eta)\Delta p_c/v_h$, with $\Delta p_c = p_0 - p_c$ and v_h the horizontal flow velocity. Considering continuity of fluid flow, we write $v_h/\Lambda \sim v_e/H$, where v_e is the rate of volume evaporation per unit area and H is the depth scale over which the vertical velocity gradient is established. For a film of particle suspension with particle radius R_p, H corresponds to the film thickness and we estimate $\Delta p_c \sim \gamma/R_p$ and $k = f(\phi)R_p^2$ (Kozeny 1927, Carman 1937), which gives $\Lambda \sim [f(\phi)(\gamma/\eta)R_pH/v_e]^{1/2}$ (Lee & Routh 2004).

A different scaling applies to a thick poroelastic medium with a pore size large enough to ensure fast advective liquid transport under a constant evaporation rate. The shrinkage and crack

fronts propagate through the medium, leading to the formation of columnar joints (Goehring 2009, Goehring et al. 2009) as shown in **Figure 4*c***. The ratio of the time for poroelastic diffusion (Λ^2/D_p) to the time for advective liquid transport (Λ/v_f) corresponds to the Péclet number, $Pe = v_f\Lambda/D_p$, where v_f corresponds to the drying front velocity. For a constant Pe, we find Λ to be inversely proportional to v_f (or the moisture flux), $\Lambda \sim v_f^{-1}$, as shown in **Figure 4*d***. When the crack front cannot propagate into the bulk due to a great toughness of the inner layer while the drying still accumulates strain, the drying outer layer can peel off, as shown in **Figure 4*e***. Such drying-induced delamination has been observed in gels (Chung et al. 2016) and muds (Allen 1986, Style et al. 2011).

4.2. Swelling of Porous Matrices of Hygroscopically Active Skeletons

We now consider porous media comprising matrices of hygroscopically active materials, e.g., networks of hydrogels and cellulose and beds of granules, such as soils, hydrogel beads, and wood particles. The voids of the matrix can range from tens of micrometers to millimeters in size. When the porous matrix is brought into contact with a favorable solvent, the liquid wicks into the voids, which deform by poroelastic deformation of the hyroscopically active skeletons. The rearrangement of the matrix in turn affects the wicking flow of liquid. As an exemplary system, **Figure 3*d*** shows the growth in height of a bed of hydrogel beads in contact with water at its bottom while confined at its sides.

A macroscopic description of the flow wicking into the swelling matrix (Masoodi & Pillai 2010) as shown in **Figure 2*d*** starts from Darcy's law, $q_x = -(k/\eta)\,\mathrm{d}p/\mathrm{d}x$ for $0 < x < L$, where q_x is the one-dimensional flux in the x-direction. The mass conservation of the liquid that can be absorbed by the solid matrix is written as $\mathrm{d}q_x/\mathrm{d}x = -S - \dot{\phi}$, where S is the absorption rate per unit volume. Here we consider a negative rate of change of the porosity, $\dot{\phi} < 0$, which is the case when the matrix is entirely or partially confined, as shown in **Figure 3*d***. Assuming $S = -b\dot{\phi}$, with b the absorption coefficient, we get $\mathrm{d}^2p/\mathrm{d}x^2 = (1-b)(\eta/k)\dot{\phi}$, which gives $p(x,t)$ satisfying such boundary conditions as $p(x=0,t) = p_0$ and $p(x=L,t) = p_0 - \gamma\kappa_m$. The velocity of the wet front, $\dot{L} = q_x/\phi|_{x=L}$, with $\phi|_{x=L}$ equal to the original porosity ϕ_0, is then given by $\dot{L} = -(1-b)\dot{\phi}/(2\phi_0)L + k\gamma\kappa_m L/(\phi_0\eta)$. Integrating with the initial condition of $L(t=0) = 0$, we get (Masoodi & Pillai 2010)

$$L = \left\{ \frac{2\gamma\kappa_m}{\phi_0\eta} \exp\left[(b-1)\frac{\phi(t)}{\phi_0}\right] \int_0^t k(t') \exp\left[(b-1)\frac{\phi(t')}{\phi_0}\right] \mathrm{d}t' \right\}^{1/2}. \qquad 15.$$

When the swelling rate of matrix matches the volumetric absorption rate, $b = 1$, Equation 15 simplifies to $L = [2\gamma\kappa_m \int_0^t k(t')\,\mathrm{d}t'/(\phi_0\eta)]^{1/2}$. Here we have assumed that the porosity ϕ and permeability k are functions of time only, independent of spatial coordinates.

To predict the wetting front velocity via Equation 15, one needs to know the temporal evolutions of ϕ and k. To this end, we need to consider the dynamic interactions of neighboring solid elements in addition to the swelling kinetics of the individual solid skeletons. For a bed of gel beads, the particles are rearranged by volume expansion, shear, and sliding (Sweijen et al. 2017), while satisfying the boundary conditions of the overall macroscopic structure. Numerical simulations can be used to fully account for the grain-scale interactions to the macroscale swelling (Kimber et al. 2012, Sweijen et al. 2016). A representative result of the height evolution of a bed of superabsorbent polymer particles is shown in **Figure 3*e***.

Alternatively, pore structures and their temporal evolutions were simplified to model the permeability and match the analytical results with experiments (Wålinder & Gardner 1999, Shi & Gardner 2000, Markl et al. 2017). Schuchardt & Berg (1991) suggested a notably simple

model for the effective capillary radius, r, of a porous structure that decreases with time due to swelling of surrounding hygroscopic skeletons, $r = r_0 - at$, where r_0 is the original radius when dry and a is the rate of constriction. Then the Poiseuille solution for such a capillary flow gives

$$L = \left(\frac{r_0\gamma}{2\eta}\right)^{1/2}\left(t - \frac{a}{r_0}t^2 + \frac{a^2}{3r_0^2}t^3\right)^{1/2}, \qquad 16.$$

where a can be adjusted to match the result with the experimental measurements that show gradual deviation from the classical $t^{1/2}$ rule of Washburn.

4.3. Swelling of Cellulosic Media

Poroelastic materials made of hygroscopically active skeletons of cellulose, such as paper and cellulose sponges, deserve separate treatment for their complicated porous network structures (Rey & Vandamme 2013, Chang et al. 2018) and transient pore coalescence behavior (Ha et al. 2018). Paper, a sheet of several cellulose fiber layers compressed in the thickness direction and stretched along a length, is a highly anisotropic material (Alava & Niskanen 2006). The wicking and swelling of paper follow Washburn-like diffusive dynamics, although the rates differ in each direction (Lee et al. 2016). Cellulose sponges exhibit isotropic swelling behavior, unlike paper, but the dynamics are quite different from those of other soft porous materials for the unique pore structure and properties. We note that bread and the cracker in **Figure 1*c***, which are made from starch, also behave similarly to cellulose sponges when wet (Ha et al. 2018).

Cellulose sponges consist of numerous microporous sheets with nanoscale thickness surrounding millimetric voids (**Figure 5*a–c***), and thus have a pseudo-bimodal pore size distribution (Kim et al. 2017). When the sheet becomes wet by water, growing micropores coalesce with

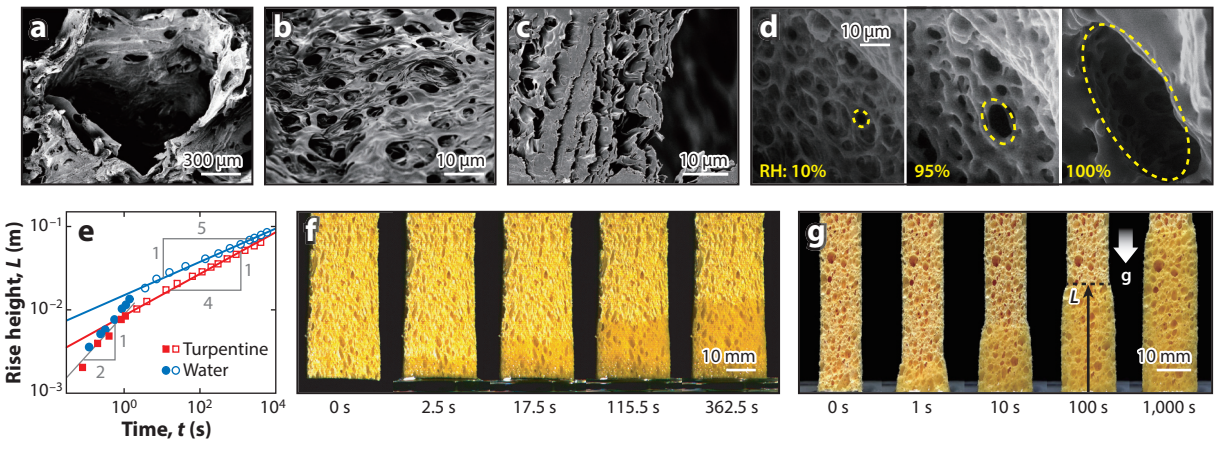

Figure 5

(*a*) Scanning electron microscopy images of a millimetric large void of the cellulose sponge. (*b*) Micropores of the sheet surrounding macro voids. (*c*) A cross section of microporous sheets. (*d*) The merging of micropores with hygroscopic expansion, imaged by environmental scanning electron microscopy. (*e*) Experimentally measured rise height of turpentine (*red squares*) and water (*blue circles*), which grows like $t^{1/2}$ in the early stages (*filled symbols*) but in the late stages behaves like $t^{1/4}$ for turpentine and $t^{1/5}$ for water (*empty symbols*). (*f*) Capillary rise of silicone oil with a viscosity of $\eta = 0.01$ Pa·s in a cellulose sponge. (*g*) Wetting and swelling of a cellulose sponge with capillary rise of water. Abbreviation: *L*, rise height; RH, relative humidity. Panels *a–e* and *g* adapted from Ha et al. (2018); panel *f* adapted from Kim et al. (2017).

their neighbors, as shown in **Figure 5*d***. Capillary imbibition in cellulose sponges situated horizontally follows the classical Washburn dynamics, so that the wet length grows like $t^{1/2}$. In contrast, capillary rise against gravity in cellulose sponges exhibits two distinct regimes (Siddique et al. 2009): The rise height L grows like $t^{1/2}$ initially but the power law changes later, as shown in **Figure 5*e***. For nonaqueous liquids (e.g., turpentine, silicone oils) that cause no swelling in the sponges (**Figure 5*f***), L grows like $t^{1/4}$ in the late stages (Kim et al. 2017). Aqueous liquids (e.g., water, water–glycerine mixtures, water–ethylene glycol mixtures) swell the sponges during ascent (**Figure 5*g***) to yield $L \sim t^{1/5}$ in the late stages. If the sponge is preswollen by water vapor without its micro and macro voids filled with liquid water, the water rise height grows like $t^{1/4}$ in the late stages, just like with nonaqueous liquids, indicating the critical role of the hygroscopic swelling in the capillary rise dynamics (Ha et al. 2018).

The abovementioned change in the power law of the capillary rise height arises when the wet front reaches Jurin's height, L_J, or the equilibrium rise height of macroscale pores. The macro voids are completely filled with infiltrating liquid for $L < L_J$, so that k and λ can be respectively scaled as R^2 and R in the definition of D_w used in Equation 2, where R is the average radius of the macro voids. The sponge that swells upon contacting an aqueous liquid stretches by $L\epsilon_h$, where ϵ_h is the hygroscopic strain of the saturated sponge, giving the total wet distance as $l_w = L(1 + \epsilon_h)$. The liquid flux into the unit cross-sectional area of a dry sponge v is balanced by the rate of expanding a wet volume, $v \approx \dot{l}_w(1 + \epsilon_h)^2$. Then $\dot{L} \approx v/\zeta$ follows, where ζ is approximately $1 + 3\epsilon_h$ for $\epsilon_h \ll 1$, which eventually leads to $L \sim [\gamma Rt/(\zeta\eta)]^{1/2}$. This scaling law explains the rise dynamics in the early stages for both nonaqueous ($\zeta = 1$) and aqueous ($\zeta > 1$) liquids.

Beyond Jurin's height, macro voids are only wet in their walls and corners for gravitational effects. The liquid rise is now driven by the capillary pressure of the micropores of average radius r, which still dominates over gravitational effects. Thus, we take $\lambda \sim r$ in the definition of D_w used in Equation 2. The primary flow path from the reservoir to the micropores is provided by the liquid hanging in corners of the macro voids, leading us to $k \sim \beta^2$, where β is the radius of corner meniscus given by the balance between capillary and hydrostatic pressure, $\gamma/\beta \sim \rho g L$. Darcy's law then gives $v \sim \gamma^3/(\eta\rho^2 g^2 r L^3)$. This allows us to obtain the scaling law for L of nonaqueous liquids in the late stages,

$$L \sim \left[\frac{\gamma^3}{\eta(\rho g)^2 r}\right]^{1/4} t^{1/4}. \qquad 17.$$

The late stages of the rise of aqueous liquids behave differently from Equation 17, which has been attributed to the merging of micropores upon wetting (**Figure 5*d***) and swelling (Ha et al. 2018). The theoretical model, $L \sim (Bt)^{1/5}$, where the coefficient B involves the physical properties of the liquid and poroelastic characteristics of the sponge, was found to be consistent with experimental measurement results using various aqueous liquids. An alternative explanation of the wetting dynamics in late stages, which involves modeling based on the water diffusion (Mirzajanzadeh et al. 2019), awaits refinement to account for the effects of swelling, the rise dynamics following the $t^{1/4}$ rule in the preswollen sponges, and the empirically observed dependence of the rise speed on the liquid properties.

5. PORO-ELASTO-CAPILLARY MORPHING OF SHEETS

We now consider global deflections of solids induced by localized swelling of soft porous materials upon wetting. Such an efficient scheme of morphing has been explored predominantly for thin sheets, whose global shapes can change easily compared to bulks through diverse modes of

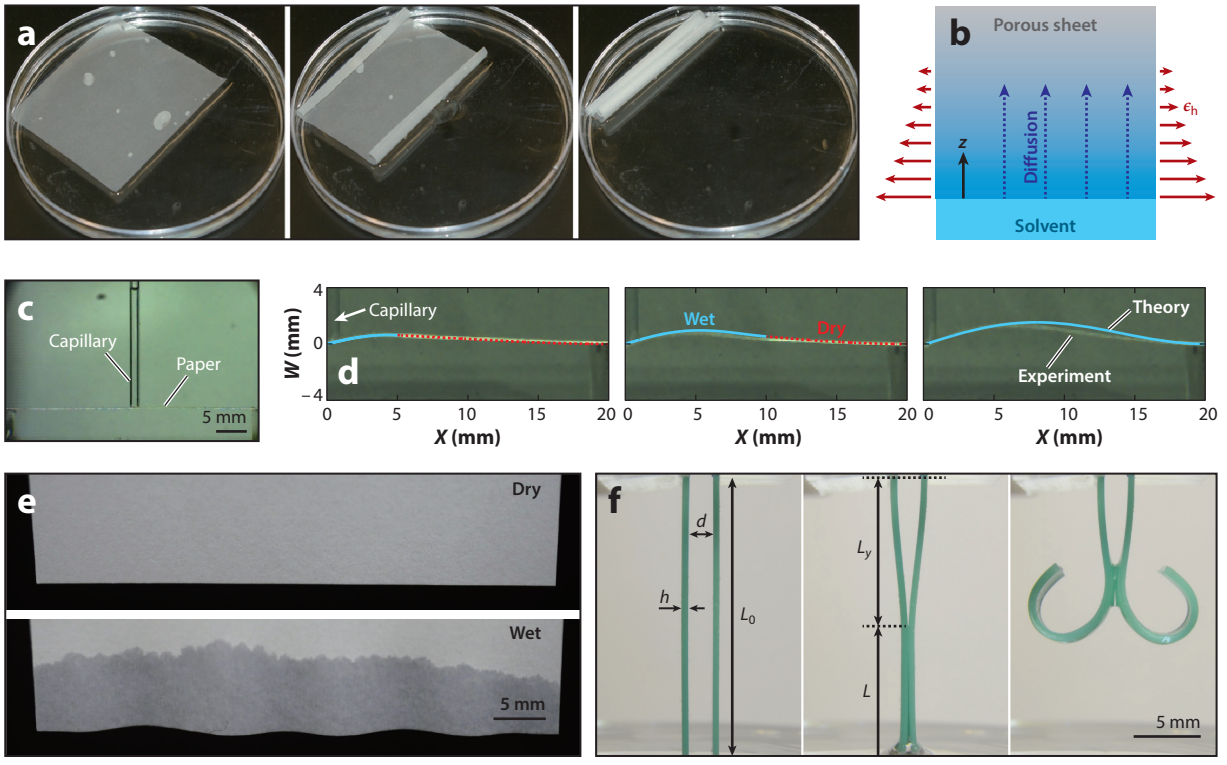

Figure 6

(*a*) A tracing paper (8×8 cm^2) that curls and rolls up when floating on water. (*b*) Schematic cross section of the porous sheet with differential swelling due to varying moisture content. (*c*) A suspended paper strip that is wetted by water from a capillary in the middle. (*d*) Comparison of experimental and theoretical results for the shape evolution of a paper strip imbibing water from a capillary tube on the left. (*e*) Wrinkling of the wet end of a copy paper. (*f*) Silicone rubber beams undergoing inward bending due to capillary rise and then outward bending due to swelling with the imbibition of silicone oil. Abbreviations: d, initial gap; ϵ_h, hygroscopic strain; h, initial thickness; L_y, length of the dry region ($L_y = L_0 - L$). Panels adapted from (*a*) Reyssat & Mahadevan (2011), (*c*,*d*) Lee et al. (2016), and (*f*) Holmes et al. (2016).

buckling, bending, wrinkling, folding, and twisting. Because the elastic response of an entire solid body as triggered by localized swelling is of primary interest, the relative scales of characteristic times for local and global deflections play an important role in the analysis.

5.1. Curling and Rolling

Differential swelling or shrinkage of sheets can shift their global shapes. Capillary imbibition occurs always from the boundary of a solid and a liquid, which inevitably gives rise to differential strains due to wetting. We first consider porous sheets that experience differential swelling by liquid absorption in thickness direction. A tracing paper floating on water, as shown in **Figure 6*a***, curls and eventually rolls up into a cylinder (Douezan et al. 2011, Reyssat & Mahadevan 2011, Perez-Cruz et al. 2017). Here, the paper swells in the wet bottom while the upper part remains dry, thus curling the porous sheet.

For dense porous media like tracing paper, the absorption of water by fibers appears to dominate over the thicknesswise wicking of water into pores surrounded by fibers. Therefore, the change in thickness with fiber expansion immediately brings about global curling of the paper.

We first assume that the tracing paper is a bilayer with a sharp interface, composed of a dry and a wet layer of thicknesses h_d and h_w and Young's moduli E_d and E_w, respectively. The curvature of the partially wet paper can be predicted using the classical theory of Timoshenko (1925). The curvature κ of the bilayer is given by

$$\kappa = \frac{\epsilon}{h} f(m, n), \qquad 18.$$

where ϵ is the thicknesswise strain in the wet layer, h is the entire thickness of the bilayer, and we have $m = h_d/h_w$, $n = E_d/E_w$, and $f = 6(1+m)^2/\{3(1+m)^2 + (1+mn)[m^2 + (mn)^{-1}]\}$. If the wet thickness grows diffusively with time, following Washburn's equation, $h_w(t) = (D_w t)^{1/2}$, we can predict the curvature evolution with time until the sheet is entirely soaked.

For dense media like tracing paper, the diffusion model given by Equation 4 has been shown to provide a theoretical prediction of sheet curvature that is closer to experimental measurements than the foregoing classical imbibition model (Reyssat & Mahadevan 2011, Perez-Cruz et al. 2017). In the diffusion model, the moisture content $\theta(z, t)$ is of interest rather than the position of wet front, $h_w(t)$. The hygroscopic strain ϵ_h now assumes a smooth gradient over the entire thickness as given by $\epsilon_h = \alpha_h \theta(z, t)$, where α_h is the hygroscopic expansion coefficient (**Figure 6*b***). The equilibrium condition in the absence of external loads gives the force, $F = \int_0^b \sigma \, dz = 0$, and the moment, $M = \int_0^b \sigma z dz = 0$, where $\epsilon = -\kappa(z - z_n) - \epsilon_h$ is the total strain, z_n is the reference plane, and $\sigma = E\epsilon$ is the local stress. Knowledge of the dependence of D_u and E on θ allows us to compute the curvature evolution with time.

The curling of plates, which swell differentially in the thickness direction in response to various external stimuli such as vapor, heat, light, and electromagnetic field, can be understood in the same theoretical framework as above. In particular, the curling of liquid-absorbing sheets was investigated in the contexts of a flower-mimicking paper–plastic bilayer dipped in water (Reyssat & Mahadevan 2009), the deployment of rolled paper architecture on water (Mulakkal et al. 2016), and the deformation of elastomer sheets contacting a favorable solvent (Holmes et al. 2011, Lucantonio & Nardinocchi 2012, Pandey & Holmes 2013). Biological tissues that change shape with moisture variation were also explained along the same lines, with examples taken from curling seed capsule layers (Witztum & Schulgasser 1995), resurrection plants (Rafsanjani et al. 2015a), and coiling seed awns of *Pelargonium* species (Jung et al. 2014).

5.2. Bending, Buckling, and Wrinkling

When a liquid wets a poroelastic hygroexpansive sheet, the stretched sheet tends to buckle under compression when confined at both ends, as shown in **Figure 6*c***. When a sheet is confined on one side and free to swell isotropically on the other side by wetting, wrinkles are formed, as in **Figure 6*e***, which shows a simplified picture of damage left on a book after spilling water on it. As the wetting front propagates with time, the bending of the buckled sheet evolves temporally, which requires us to simultaneously consider the rates of lengthwise capillary imbibition and elastic response.

For the porous sheet in **Figure 6*c***, a filter paper, we assume the capillary imbibition governs the water transport. The thicknesswise swelling and the consequent softening (reduction of Young's modulus) of the wet portion occur much faster than the lengthwise imbibition. Thus, the global deflection of the sheet can be obtained by assuming the wet portion to have a fixed thickness (maximum swelling thickness) and Young's modulus. As the bending process is decoupled from the hygroexpansive swelling dynamics, we can set up geometrically nonlinear postbuckling equations of force and moment equilibrium and geometric compatibility for wet and dry domains, whose

boundary moves with a prescribed imbibition velocity. The equations can be solved numerically with pertinent conditions at the boundaries and the interfaces of wet and dry domains to give the temporal evolution of the shape of the sheet in the course of capillary imbibition (**Figure 6*d***) (Lee et al. 2016).

The magnitude of deflection ξ and curvature κ of the sheet can be estimated using scaling analysis as functions of the hygroexpansive strain ϵ_h, the initial length L_0, and the wetted length, $L = l(t)L_0$. The sheet is stretched by $\Gamma \sim \epsilon_h l L_0$ in the wet domain, which is accommodated by deflection due to buckling. With $y' = dy/dx$, we write $\Gamma \sim \int_0^{L_0} [(1 + y'^2)^{1/2} - 1]\, dx \sim y'^2 L_0$ for $|y'| \ll 1$. Because of $y' \sim \xi/L_0$, we get $\xi \sim (\epsilon_h l)^{1/2}$ and $\kappa \sim y'/L \sim (\epsilon_h l)^{1/2}/L = (\epsilon_h/l)^{1/2}/L_0$.

This lengthwise imbibition is an easy way to propagate the mechanical response of a sheet to an external stimulus from one end to the other, which was used to control the morphology of long actuators (Lee et al. 2010) and to change the shape of a sagged fabric from that of the Bernoulli catenary (Monaenkova et al. 2012). It was found that poroelastic sheets of gel surrounded by a solvent wrinkle rather than buckle under compression, with the wavelength dependent on the permeability, the flexural modulus of the gel, and the viscosity of the solvent (Leocmach et al. 2015).

5.3. Morphing of Capillary Channels

When a liquid wicks between wettable elastic sheets, the capillary force acting along the three-phase contact line and the force due to negative gauge pressure on the wetted area deflect the sheets to reduce the gap, as shown in **Figure 1*b*** (Bico et al. 2004, Kim & Mahadevan 2006). When the sheets are wettable and poroelastic, they change their volume and stiffness when absorbing the liquid flowing between them, thereby further altering the morphology of the capillary channels. **Figure 6*f*** shows that such sheets initially bend inward as dominated by elasto-capillarity and later curl outward as they become swollen with diffused solvent (Holmes et al. 2016).

For the materials system employed in the experiments shown in **Figure 6*f***, the capillary rise between the elastomer plates, of the initial thickness h and gap d, occurs much faster than the thicknesswise swelling owing to solvent diffusion. The initial inward bending of plates and their consequent adhesion follows the classical elasto-capillary theory. The length of a dry region, L_y, can be obtained by minimizing the sum of the elastic energy of the deformed plates and the interfacial energy, $L_y \sim (dl_e)^{1/2}$, where l_e is the elasto-capillary length defined as $l_e = (B/\gamma)^{1/2}$ (Cohen & Mahadevan 2003). Here, $B = Eh^3/[12(1 - \nu^2)]$ is the bending stiffness per unit width of the plates.

The effects of (slow) solvent diffusion and consequent swelling manifest after (fast) elasto-capillary rise of the solvent. The gradient of swelling established in the thickness direction causes the plates to curl apart while maintaining their capillary adhesion in the middle (the right subpanel in **Figure 6*f***). As the curling is resisted by the surface tension of the solvent, the critical curvature of the plates at the instant of peeling is scaled as l_e^{-1} (Holmes et al. 2016), where l_e should account for the change of B due to solvent absorption.

Nasouri et al. (2019) considered theoretically the rise of water between poroelastic paper sheets, where the thicknesswise swelling by solvent imbibition is much faster than the elasto-capillary rise, while the lengthwise imbibition within the sheet is much slower than the elasto-capillary rise. Then the dynamics are governed by the capillary flows between the Hookean sheets (Duprat et al. 2011), whose bending stiffness immediately changes when wet because of softening (reduction of E) and swelling (increase of h). Wong et al. (2016) showed that the elasto-capillary wrapping of a water droplet by thin wettable films (Py et al. 2007) was promoted by using a superhydrophilic poroelastic nanofibrous layer backed by a sealing layer. This wrapping response was made to propagate along a predetermined direction to guide the liquid flow.

6. SUMMARY

We have reviewed the recent advances in understanding and exploring deformations of soft porous solids due to capillary imbibition of liquids. After introducing fundamental physical principles associated with poro-elasto-capillarity, we have treated the swelling and shrinkage of bulk poroelastic media. Then we have considered various morphing modes of porous sheets, which are induced by localized wetting and swelling of soft porous materials.

In reviewing the physical principles, we have encountered various diffusion or diffusion-like equations, and the corresponding diffusivities. We summarize the diffusivities in order to help readers clearly distinguish their physical significances and use them discerningly. The term D_w in Equation 2 is for the capillary wicking through porous media with constant permeability and meniscus curvature. In Equation 4, D_u designates the diffusivity of moisture content in a partially saturated zone. In Equation 5, D_m is the diffusivity of fluid molecules through porous media. In Equation 10, D_p corresponds to the diffusivity for pressure equilibration via fluid transport in fully saturated poroelastic media. Although D_w and D_u directly involve the liquid–gas surface tension coefficient, D_m and D_p can also play a role in poro-elasto-capillarity when the skeletons of the poroelastic matrices, like gels and cellulose fibers, swell by absorbing liquid.

Recent growing interest in soft robotics and bio-inspired engineering of poroelastic materials and tissues are anticipated to lead innovations in the understanding, exploration, and control of the morphing of soft porous solids. The interactions of soft materials with wet environments will play essential roles in future applications in health, water, energy, and food.

FUTURE ISSUES

1. The transport of liquids in partially saturated zones deserves further quantitative investigation into the role of capillarity, surface adsorption, and local condensation.
2. Prediction and control of the morphing of poroelastic matrices of hygroscopically active skeletons remain rich problems that require us to consider porous flows and poroelastic and tribological responses of skeletons on multiple scales.
3. We need to continuously learn from biological creatures' ingenious tactics to actuate in an optimal manner their poroelastic tissues in response to external stimuli.
4. Efficient schemes to trigger drastic shape changes of three-dimensional soft porous bulks with localized poro-elasto-capillary responses will have a significant impact on soft robotics and biomimetics.

DISCLOSURE STATEMENT

The authors are not aware of any biases that might be perceived as affecting the objectivity of this review.

ACKNOWLEDGMENTS

We are grateful to Prof. Detlef Lohse for encouragement, Prof. L. Mahadevan for stimulating discussions, and Profs. Wonjung Kim and Jeong-Yun Sun and Dr. Yeonsu Jung for helpful comments. This work was supported by National Research Foundation of Korea (grant number 2018-052541) via SNU IAMD (Seoul National University Institute of Advanced Machines and Design).

LITERATURE CITED

Adam NK. 1930. *Physics and Chemistry of Surfaces*. London: Oxford Univ. Press

Adamson AW, Gast AP. 1997. *Physical Chemistry of Surfaces*. New York: Wiley. 6th ed.

Adler PM, Brenner H. 1988. Multiphase flow in porous media. *Annu. Rev. Fluid Mech.* 20:35–59

Alava M, Niskanen K. 2006. The physics of paper. *Rep. Prog. Phys.* 69:669–723

Allain C, Limat L. 1995. Regular patterns of cracks formed by directional drying of a collodial suspension. *Phys. Rev. Lett.* 74:2981–84

Allen JRL. 1986. On the curl of desiccation polygons. *Sediment. Geol.* 46:23–31

Bacchin P, Brutin D, Davaille A, Di Giuseppe E, Chen XD, et al. 2018. Drying colloidal systems: laboratory models for a wide range of applications. *Eur. Phys. J. E* 41:94

Bal K, Fan J, Sarkar MK, Ye L. 2011. Differential spontaneous capillary flow through heterogeneous porous media. *Int. J. Heat Mass Transf.* 54:3096–99

Bear J. 1972. *Dynamics of Fluids in Porous Media*. New York: Elsevier

Bell JM, Cameron FK. 1906. The flow of liquids through capillary spaces. *J. Phys. Chem.* 10:658–74

Bertrand T, Peixinho J, Mukhopadhyay S, MacMinn CW. 2016. Dynamics of swelling and drying in a spherical gel. *Phys. Rev. Appl.* 6:064010

Bico J, Reyssat É, Roman B. 2018. Elastocapillarity: when surface tension deforms elastic solids. *Annu. Rev. Fluid Mech.* 50:629–59

Bico J, Roman B, Moulin L, Boudaoud A. 2004. Elastocapillary coalescence in wet hair. *Nature* 432:690

Bico J, Tordeux C, Quéré D. 2001. Rough wetting. *Europhys. Lett.* 55:214–20

Biot MA. 1941. General theory of three dimensional consolidation. *J. Appl. Phys.* 12:155–64

Bou Zeid W, Vicente J, Brutin D. 2013. Influence of evaporation rate on cracks' formation of a drying drop of whole blood. *Colloids Surf. A* 432:139–46

Boyle R. 1662. *New Experiments Physico-Mechanicall, Touching the Spring of the Air, and Its Effects*. Oxford: H. Hall

Carman PC. 1937. Fluid flow through granular beds. *Trans. Inst. Chem. Eng.* 15:150–67

Chang S, Seo J, Hong S, Lee DG, Kim W. 2018. Dynamics of liquid imbibition through paper with intra-fiber pores. *J. Fluid Mech.* 845:36–50

Chen X, Mahadevan L, Driks A, Sahin O. 2014. *Bacillus* spores as building blocks for stimuli-responsive materials and nanogenerators. *Nat. Nanotechnol.* 9:137–41

Cheng AEH. 2016. *Poroelasticity*. Cham, Switz.: Springer

Childs EC, Collis-George N. 1950. The permeability of porous materials. *Proc. R. Soc. A* 201:392–405

Chung JY, Regev I, Mahadevan L. 2016. Spontaneous exfoliation of a drying gel. *Soft Matter* 12:7855–62

Cohen AE, Mahadevan L. 2003. Kinks, rings, and rackets in filamentous structures. *PNAS* 100:12141–46

Coussy O. 2007. Revisiting the constitutive equations of unsaturated porous solids using a Lagrangian saturation concept. *Int. J. Numer. Anal. Methods Geomech.* 31:1675–94

Cuerto-Felgueroso L, Juanes R. 2008. Nonlocal interface dynamics and pattern formation in gravity-driven unsaturated flow through porous media. *Phys. Rev. Lett.* 101:244504

Darcy H. 1856. *Les Fontaines Publiques de la Ville de Dijon*. Paris: Victor Dalmont

Dawson C, Vincent JFV, Rocca AM. 1997. How pine cones open. *Nature* 390:668

de Gennes PG. 1985. Wetting: statics and dynamics. *Rev. Mod. Phys.* 57:827–63

de Gennes PG, Brochard-Wyart F, Quéré D. 2004. *Capillarity and Wetting Phenomena*. New York: Springer

Dervaux J, Couder Y, Guedeau-Boudeville MA, Ben Amar M. 2011. Shape transition in artificial tumors: from smooth buckles to singular creases. *Phys. Rev. Lett.* 107:018103

Doi M. 2009. Gel dynamics. *J. Phys. Soc. Jpn.* 78:052001

Douezan S, Wyart M, Brochard-Wyart F, Cuvelier D. 2011. Curling instability induced by swelling. *Soft Matter* 7:1506–11

Dufresne ER, Stark DJ, Greenblatt NA, Cheng JX, Hutchinson JW, et al. 2006. Dynamics of fracture in drying suspensions. *Langmuir* 22:7144–47

Dumais J, Forterre Y. 2012. "Vegetable dynamicks": the role of water in plant movements. *Annu. Rev. Fluid Mech.* 44:453–78

Duprat C, Aristoff JM, Stone HA. 2011. Dynamics of elastocapillary rise. *J. Fluid Mech.* 679:641–54
Duprat C, Protiére S, Beebe AY, Stone HA. 2012. Wetting of flexible fibre arrays. *Nature* 482:510–13
Fisher L. 1999. Physics takes the biscuit. *Nature* 397:469
Flory PJ. 1953. *Principles of Polymer Chemistry*. Ithaca, NY: Cornell Univ. Press
Ghezzehei TA, Or D. 2000. Dynamics of soil aggregate coalescence governed by capillary and rheological processes. *Water Resour. Res.* 36:367–79
Giorgiutti-Dauphiné F, Pauchard L. 2014. Elapsed time for crack formation during drying. *Eur. Phys. J. E* 37:39
Goehring L. 2009. Drying and cracking mechanisms in a starch slurry. *Phys. Rev. E* 80:036116
Goehring L, Mahadevan L, Morris SW. 2009. Nonequilibrium scale selection mechanism for columnar jointing. *PNAS* 106:387–92
Gorce JB, Hewitt IJ, Vella D. 2016. Capillary imbibition into converging tubes: beating Washburn's law and the optimal imbibition of liquids. *Langmuir* 32:1560–67
Gummerson RJ, Hall C, Hoff WD, Hawkes R, Holland GN, Moore WS. 1979. Unsaturated water flow within porous materials observed by NMR imaging. *Nature* 281:56–57
Ha J, Kim J, Jung Y, Yun G, Kim DN, et al. 2018. Poro-elasto-capillary wicking of cellulose sponges. *Sci. Adv.* 4:eaao7051
Hall C, Tse TKM. 1986. Water movement in porous building materials—VII. The sorptivity of mortars. *Build. Environ.* 21:113–18
Hines L, Petersen K, Lum GZ, Sitti M. 2017. Soft actuators for smallscale robotics. *Adv. Mater.* 29:1603483
Hoberg TB, Verneuil E, Hosoi AE. 2014. Elastocapillary flows in flexible tubes. *Phys Fluids* 26:122103
Holmes DP, Brun PT, Pandey A, Protière S. 2016. Rising beyond elastocapillarity. *Soft Matter* 12:4886–90
Holmes DP, Roché M, Sinha T, Stone HA. 2011. Bending and twisting of soft materials by non-homogenous swelling. *Soft Matter* 7:5188–93
Hu C, Pané S, Nelson BJ. 2018. Soft micro- and nanorobotics. *Annu. Rev. Control Robot. Auton. Syst.* 1:53–75
Hu Y, Zhao X, Vlassak JJ, Suo Z. 2010. Using indentation to characterize the poroelasticity of gels. *Appl. Phys. Lett.* 96:121904
Johnson DL. 1982. Elastodynamics of gels. *J. Chem. Phys.* 77:1531–39
Jung W, Kim W, Kim HY. 2014. Self-burial mechanics of hygroscopically responsive awns. *Integr. Comp. Biol.* 54:1034–42
Jurin J. 1718. An account of some experiments shown before the Royal Society; with an enquiry into the cause of the ascent and suspension of water in capillary tubes. *Philos. Trans. R. Soc. Lond.* 30:739–47
Kalnin JR, Kotomin E. 1998. Modified Maxwell-Garnett equation for the effective transport coefficients in inhomogeneous media. *J. Phys. A* 31:7227–34
Karlsson JO, Andersson M, Berntsson P, Chihani T, Gatenholm P. 1998. Swelling behavior of stimuli-responsive cellulose fibers. *Polymer* 39:3589–95
Keck S. 1969. Mechanical alteration of the paint film. *Stud. Conserv.* 14:9–30
Kim HY. 2007. On thermocapillary propulsion of microliquid slug. *Nanosc. Microsc. Therm.* 11:351–62
Kim HY, Mahadevan L. 2006. Capillary rise between elastic sheets. *J. Fluid Mech.* 548:141–50
Kim J, Ha J, Kim HY. 2017. Capillary rise of non-aqueous liquids in cellulose sponges. *J. Fluid Mech.* 818:R2
Kim J, Moon MW, Kim HY. 2016. Dynamics of hemiwicking. *J. Fluid Mech.* 800:57–71
Kim J, Moon MW, Lee KR, Mahadevan L, Kim HY. 2011. Hydrodynamics of writing with ink. *Phys. Rev. Lett.* 107:264501
Kimber JA, Kazarian SG, Štěpánek F. 2012. Modelling of pharmaceutical tablet swelling and dissolution using discrete element method. *Chem. Eng. Sci.* 69:394–403
Kindle EM. 1917. Some factors affecting the development of mud-cracks. *J. Geol.* 25:135–44
Kozeny J. 1927. Über kapillare Leitung des Wassers im Boden. *Stizungsber. Akad. Wiss. Wien* 136:271–306
Laloui L, Ferrari A, Li C, Eichenberger J. 2016. Hydro-mechanical analysis of volcanic ash slopes during rainfall. *Géotechnique* 66:220–31

Lee H, Xia C, Fang NX. 2010. First jump of microgel: actuation speed enhancement by elastic instability. *Soft Matter* 6:4342–45

Lee M, Kim S, Kim HY, Mahadevan L. 2016. Bending and buckling of wet paper. *Phys. Fluids* 28:042101

Lee WP, Routh AF. 2004. Why do drying films crack? *Langmuir* 20:9885–88

Leocmach M, Nespoulous M, Manneville S, Gibaud T. 2015. Hierarchical wrinkling in a confined permeable biogel. *Sci. Adv.* 1:e1500608

Liu M, Suo S, Wu J, Gan Y, Hanaor DA, Chen CQ. 2018. Tailoring porous media for controllable capillary flow. *J. Colloid Interf. Sci.* 539:379–87

Lucantonio A, Nardinocchi P. 2012. Reduced models of swelling-induced bending of gel bars. *Int. J. Solids Struct.* 49:1399–405

Lucas R. 1918. Über das Zeitgesetz des kapillaren Aufstiegs von Flüssigkeiten. *Kolloid Z.* 23:15–22

Markl D, Yassin S, Wilson DI, Goodwin DJ, Anderson A, Zeitler JA. 2017. Mathematical modelling of liquid transport in swelling pharmaceutical immediate release tablets. *Int. J. Pharm.* 526:1–10

Masoodi R, Pillai KM. 2010. Darcy's law–based model for wicking in paperlike swelling porous media. *AIChE J.* 56:2257–67

Mirzajanzadeh M, Deshpande VS, Fleck NA. 2019. Water rise in a cellulose foam: By capillary or diffusional flow? *J. Mech. Phys. Solids* 124:206–19

Monaenkova D, Andrukh T, Kornev KG. 2012. Wicking of liquids into sagged fabrics. *Soft Matter* 8:4725–30

Mulakkal MC, Seddon AM, Whittell G, Manners I, Trask RS. 2016. 4D fibrous materials: characterising the deployment of paper architectures. *Smart Mater. Struct.* 25:095052

Nasouri B, Thorne B, Elfring GJ. 2019. Dynamics of poroelastocapillary rise. *J. Fluids Struct.* 85:220–28

Nielsen AF. 1972. Gamma-ray-attenuation used for measuring the moisture content and homogeneity of porous concrete. *Build. Sci.* 7:257–63

Obara N, Okumura K. 2012. Imbibition of a textured surface decorated by short pillars with rounded edges. *Phys. Rev. E* 86:020601

Or D, Tuller M, Wraith JM. 2005. Water potential. In *Encyclopedia of Soils in the Environment*, ed. D Hillel, C Rosenzweig, D Powlson, K Scow, M Singer, et al., pp. 270–77. Oxford: Academic

Pandey A, Holmes DP. 2013. Swelling-induced deformations: a materials-defined transition from macroscale to microscale deformations. *Soft Matter* 9:5524–28

Park SJ, Weon BM, Lee JS, Lee J, Kim J, Je JH. 2014. Visualization of asymmetric wetting ridges on soft solids with X-ray microscopy. *Nat. Commun.* 5:4369

Paulsen JD, Démery V, Santangelo CD, Russell TP, Davidovitch B, Menon N. 2015. Optimal wrapping of liquid droplets with ultrathin sheets. *Nat. Mater.* 14:1206–9

Peev G, Tzibranska I. 1997. Modelling of fluid–solid mass transfer in packed beds: cases of nonuniform particles and concentration dependent internal diffusivity. *Chem. Eng. Process.* 36:317–25

Perez-Cruz A, Stiharu I, Dominguez-Gonzalez A. 2017. Nonlinear imbibition influence on the hygromechanical bending response of paper due to its interaction with water. *Int. J. Nonlin. Mech.* 97:89–95

Philip JR. 1970. Flow in porous media. *Annu. Rev. Fluid Mech.* 2:177–204

Ponomarenko A, Quéré D, Clanet C. 2011. A universal law for capillary rise in corners. *J. Fluid Mech.* 666:146–54

Py C, Reverdy P, Doppler L, Bico J, Roman B, Baroud CN. 2007. Capillary origami: spontaneous wrapping of a droplet with an elastic sheet. *Phys. Rev. Lett.* 98:156103

Rafsanjani A, Brulé V, Western TL, Pasini D. 2015a. Hydro-responsive curling of the resurrection plant *Selaginella lepidophylla*. *Sci. Rep.* 5:8064

Rafsanjani A, Derome D, Carmeliet J. 2015b. Poromechanical modeling of moisture induced swelling anisotropy in cellular tissues of softwoods. *RSC Adv.* 5:3560–66

Rey J, Vandamme M. 2013. On the shrinkage and stiffening of a cellulose sponge upon drying. *J. Appl. Mech.* 80:020908

Reyssat E, Mahadevan L. 2009. Hygromorphs: from pine cones to biomimetic bilayers. *J. R. Soc. Interface* 6:951–57

Reyssat E, Mahadevan L. 2011. How wet paper curls. *Europhys. Lett.* 93:54001

Reyssat M, Courbin L, Reyssat E, Stone HA. 2008. Imbibition in geometries with axial variations. *J. Fluid Mech.* 615:335–44

Reyssat M, Sangne LY, van Nierop EA, Stone HA. 2009. Imbibition in layered systems of packed beads. *Europhys. Lett.* 86:56002

Richards LA. 1931. Capillary conduction of liquids through porous mediums. *J. Appl. Phys.* 1:318–33

Saguy IS, Marabi A, Wallach R. 2005. Liquid imbibition during rehydration of dry porous foods. *Innov. Food Sci. Emerg. Technol.* 6:37–43

Scherer GW. 1989. Drying gels: VIII. Revision and review. *J. Non-Cryst. Solids* 109:171–82

Scherer GW. 1990. Stress and fracture during drying of gels. *J. Non-Cryst. Solids* 121:104–9

Schuchardt DR, Berg JC. 1991. Liquid transport in composite cellulose—superabsorbent fiber networks. *Wood Fiber Sci.* 23:342–57

Shi SQ, Gardner DJ. 2000. A new model to determine contact angles on swelling polymer particles by the column wicking method. *J. Adhes. Sci. Technol.* 14:301–14

Shin B, Ha J, Lee M, Park K, Park GH, et al. 2018. Hygrobot: a self-locomotive ratcheted actuator powered by environmental humidity. *Sci. Robot.* 3:eaar2629

Siddique JI, Anderson DM, Bondarev A. 2009. Capillary rise of a liquid into a deformable porous material. *Phys. Fluids* 21:013106

Singh K, Jung M, Brinkmann M, Seemann R. 2019. Capillary-dominated fluid displacement in porous media. *Annu. Rev. Fluid Mech.* 51:429–49

Skotheim JM, Mahadevan L. 2004. Dynamics of poroelastic filaments. *Proc. R. Soc. Lond. A* 460:1995–2020

Skotheim JM, Mahadevan L. 2005. Physical limits and design principles for plant and fungal movements. *Science* 308:1308–10

Smith DM, Scherer GW, Anderson JM. 1995. Shrinkage during drying of silica gel. *J. Non-Cryst. Solids* 188:191–206

Sojoudi H, Kim S, Zhao H, Annavarapu RK, Mariappan D, et al. 2017. Stable wettability control of nanoporous microstructures by iCVD coating of carbon nanotubes. *ACS Appl. Mater. Interfaces* 9:43287–99

Song KM, Mitchell J, Jaffel H, Gladden LF. 2011. Magnetic resonance imaging studies of spontaneous capillary water imbibition in aerated gypsum. *J. Phys. D* 44:115403

Style PW, Peppin SSL, Cocks ACF. 2011. Mud peeling and horizontal crack formation in drying clays. *J. Geophys. Res.* 116:F01025

Sweijen T, Chareyre B, Hassanizadeh SM, Karadimitriou NK. 2017. Grain-scale modelling of swelling granular materials; application to super absorbent polymers. *Powder Technol.* 318:411–22

Sweijen T, Nikooee E, Hassanizadeh SM, Chareyre B. 2016. The effects of swelling and porosity change on capillarity: DEM coupled with a pore-unit assembly method. *Transp. Porous Media* 113:207–26

Tanaka H, Tomita H, Takasu A, Hayashi T, Nishi T. 1992. Morphological and kinetic evolution of surface patterns in gels during the swelling process: evidence of dynamic pattern ordering. *Phys. Rev. Lett.* 68:2794–97

Tanaka T, Fillmore DJ. 1979. Kinetics of swelling of gels. *J. Chem. Phys.* 70:1214–18

Terzaghi K. 1925. *Erdbaumechanik auf bodenphysikalischer Grundanlage*. Vienna: Deuticke

Timoshenko S. 1925. Analysis of bi-metal thermostats. *J. Opt. Soc. Am.* 11:233–55

Uzuoka R, Borja RI. 2012. Dynamics of unsaturated poroelastic solids at finite strain. *Int. J. Numer. Anal. Geomech.* 36:1535–73

Wålinder MEP, Gardner DJ. 1999. Factors influencing contact angle measurements on wood particles by column wicking. *J. Adhes. Sci. Technol.* 13:1363–74

Wang HF. 2000. *Theory of Linear Poroelasticity*. Princeton, NJ: Princeton Univ. Press

Washburn EW. 1921. The dynamics of capillary flow. *Phys. Rev.* 17:273–83

Wijmans JG, Baker RW. 1995. The solution-diffusion model: a review. *J. Membr. Sci.* 107:1–21

Wittmann FH. 1976. On the action of capillary pressure in fresh concrete. *Cem. Concr. Res.* 6:49–56

Witztum A, Schulgasser K. 1995. The mechanics of seed expulsion in Acanthaceae. *J. Theor. Biol.* 176:531–42

Woignier T, Phalippou J, Vacher R. 1989. Parameters affecting elastic properties of silica aerogels. *J. Mater. Res.* 4:688–92

Wong WS, Li M, Nisbet DR, Craig VS, Wang Z, Tricoli A. 2016. Mimosa origami: a nanostructure-enabled directional self-organization regime of materials. *Sci. Adv.* 2:e1600417

Xu P, Yu B. 2008. Developing a new form of permeability and Kozeny–Carman constant for homogeneous porous media by means of fractal geometry. *Adv. Water Resour.* 31:74–81

Yoon J, Cai S, Suo Z, Hayward RC. 2010. Poroelastic swelling kinetics of thin hydrogel layers: comparison of theory and experiment. *Soft Matter* 6:6004–12

Young T. 1805. III. An essay on the cohesion of fluids. *Philos. Trans. R. Soc. Lond.* 95:65–87